Low-energy dissociative electron attachment to CF_{2}

S. T. Chourou, Å. Larson, and A. E. Orel

Phys. Rev. A **92**, 022702 — Published 6 August 2015

DOI: 10.1103/PhysRevA.92.022702

Low Energy Dissociative Electron Attachment to CF_2

S. T. Chourou[1], Å. Larson[2] and A. E. Orel[1]

[1]University of California, Davis, Davis CA 95616 USA [2]Stockholm University, S-106 91 Stockholm, Sweden

We present the results of a theoretical study of dissociative electron attachment (DEA) of low-energy electrons to CF_2. We carried out electron scattering calculations using the complex Kohn variational method at the static-exchange and relaxed Self-Consistent Field (SCF) level at the equilibrium geometry and compare our differential cross sections to other results. We then repeated these calculations as a function of the three internal degrees of freedom to obtain the resonance energy surfaces and autoionization widths. We use this data as input to form the Hamiltonian relevant to the nuclear dynamics. The multidimensional wave equation is solved using the Multi-Configuration Time-Dependent Hartree (MCTDH) approach within the local approximation.

PACS numbers:

I. INTRODUCTION

In the processing of semiconductor devices, fluorocarbon plasmas are often used to etch silicon surfaces [1, 2]. The gases currently used in the plasma production of microelectronic devices have been shown to have a strong greenhouse effect. CF_3I and C_2F_4 have been proposed as alternate feedstock gases [3]. Although the feed gas is non-reactive, under electron bombardment it fragments to produce reactive species such as CF, CF_2 and CF_3 radicals and the corresponding ions. Electron collision cross sections for these transient, reactive species are difficult to measure experimentally. Therefore, *ab initio* theory can be of value in estimating the cross sections that are needed in large-scale simulations of these processing plasmas [4, 5]. It is important to identify not only the cross sections but also the branching ratios into the various fragment channels following dissociation. These quantities are critical in modeling the behavior of the feedstock gases in a plasma environment [6].

One question that has arisen in these plasmas is the source of F^-. It had originally been predicted that dissociative electron attachment to CF

$$CF + e^- \rightarrow (CF)^{-*} \rightarrow C + F^-$$

would be efficient [7, 8]. Further calculations [9] showed that although as found in the previous studies, the anion curve crossed the neutral near the equilibrium geometry, at the energies needed for dissociation [7, 8], the cross section was extremely small and significant vibrational excitation was needed to produce any significant F^- product. It was also proposed the dissociative electron attachment to CF_2

$$CF_2 + e^- \rightarrow (CF_2)^{-*} \rightarrow CF + F^-$$

might be efficient. R-matrix calculations were carried out at several internuclear separations, but no dynamics for the dissociation were calculated [8, 10]. These calculations indicate the existence of at least one anion resonance $^2B_1$ ($^2A''$) which crosses the neutral and predicted the dissociative attachment cross section to be large. Later calculations [11] computed differential cross sections that compared well to experiments. These calculations at the static exchange level found a single resonance at low energy unbound at the equilibrium geometry of the ground state. However, when a static-exchange plus polarization calculation was performed, which correctly balances the anion and target correlation, the anion was found to be bound. This is in agreement with photodetachment spectroscopy experiments [12] that found the CF_2^- anion to be bound. In addition, an experiment [13] which measured the cross section for the dissociative electron attachment to CF_2 found it to be no greater than $\sim 5 \cdot 10^{-20} cm^2$. More recently [14], an experimental study of dissociative electron attachment to a number of fluorocarbon radicals found that the process yielded F^- with low efficiency (less than 2%) except in the case of CF_2 where no attachment was observed.

In this paper we present our calculations on the dissociative electron attachment to CF_2. We first describe the electron scattering calculations performed to determine the resonant states and construct the complex potential energy surfaces. We compare our differential electron scattering calculations with previous theoretical and experimental results. We discuss the computation of the nuclear dynamics of CF_2^{-*}. Finally, we present our results for the DEA cross section.

II. ELECTRON SCATTERING CALCULATIONS

We use the complex Kohn variational method [15] to describe the electron scattering from the neutral. This method has been described elsewhere so only a summary will be presented. The $(n+1)$-electron scattering wavefunction for fixed nuclei positions represented collectively by the vector $\mathbf{Q}$ is written as:

$$\Psi_{el}^{\lambda}(\mathbf{r}^{n+1};\mathbf{Q}) = \hat{A}\left[\sum_{\lambda'} \phi_{el}^{\lambda'}(\mathbf{r}^{n};\mathbf{Q}) F^{\lambda\lambda'}(\vec{r}_{n+1};k)\right] + \sum_{\mu} d_{\mu}^{\lambda} \mathbf{\Theta}_{\mu}(\mathbf{r}^{n+1};\mathbf{Q}) \quad (1)$$

where $\mathbf{r}^{n+1} = (\vec{r}_1, \vec{r}_2, ..., \vec{r}_{n+1})$ is the $(n+1)$-electronic coordinates vector and $\hat{A}$ is the antisymmetrizing operator. The first sum is denoted as the P-space portion of the wave function and runs over the energetically open target states. In this case, only one channel was open. The function $\phi_{el}^{\lambda}(\mathbf{r}^n; \mathbf{Q})$ is the target n-electron ground state in the irreducible representation λ with the nuclei clamped at $\mathbf{Q}$. The second term, denoted as the Q-space portion of the wave function, contains the functions $\mathbf{\Theta}_{\mu}$, which are square-integrable $n+1$ configuration state functions (CSFs) which are used to describe short-range correlations and the effects of closed channels. $F^{\lambda\lambda'}(\vec{r}_{n+1}; k)$ is the scattering electron's wave function at position $\vec{r}$ and momentum k, which is further expanded to match asymptotic boundary conditions:

$$F^{\lambda\lambda'}(\vec{r}; k) = \sum_i c_i^{\lambda\lambda'} u_i(\vec{r}) \quad + \tag{2}$$

$$\sum_{lm} \left[f_l^{\lambda}(kr)\delta_{ll'}\delta_{mm'}\delta_{\lambda\lambda'} + T_{ll'mm'}^{\lambda\lambda'}(k) h_l^{+\lambda}(kr) \right] Y_{lm}(\hat{r})/r$$

where the $\{u_i\}$ are square-integrable functions, $\{f_l^{\lambda}\}$ and $\{h_l^{+\lambda}\}$ are respectively the regular Ricatti-Bessel and the outgoing Hankel functions and Y_{lm} are the normalized spherical harmonics. Angular momenta up to $l = 6$ and $|m| = 4$ are included in the calculation.

By inserting the trial wave function into the complex Kohn functional [15], the unknown coefficients in the trial wave function, d_{μ}^{λ}, $c_i^{\lambda\lambda'}$ and $T_{ll'mm'}^{\lambda\lambda'}$ can be optimized. The terms $T_{ll'mm'}^{\lambda\lambda'}$ are the T-matrix elements that determine the eigenphase sums as a function of the electron's collision energy. The eigenphase sums were fit to the Breit-Wigner form [16],

$$\delta(\frac{k^2}{2}) = \arctan\left(\frac{\Gamma/2}{\epsilon - \frac{k^2}{2}}\right) + \delta_{\text{bkgd}}(\frac{k^2}{2}); \tag{3}$$

where ϵ, Γ are the corresponding parameters to be determined and δ_{bkgd} is the background phase shift taken to be a slowly varying function of the electron energy.

We performed calculations at two levels. In all calculations the carbon and flourine atoms were described using a triple-zeta-plus-polarization (TZP) function basis set [17] which is then augmented with one s with exponent 0.01 and one p function with exponent 0.09. The first calculation was carried out at the static exchange level. At this level a SCF wavefunction is used for the target wave function, $\phi_{el}^{\lambda}(\mathbf{r}^n; \mathbf{Q})$. In the second level of calculations, a static exchange plus polarization (SEP) calculation was run with a relaxed SCF (RSCF) wavefunction, that is, including all symmetry preserving single excitations from the occupied target orbitals into all unoccupied orbitals, is used. This has been used in previous studies [9] and found to yield a balanced description of the neutral and anion. This leads to 9075 configurations in $^2\text{A}''$, the symmetry that includes the resonance.

We have chosen to work in the internal coordinate system shown in Figure 1. The coordinates r_1 and r_2 represent the distance between the two fluorine atoms and the carbon atom, and θ is the F–C–F angle.

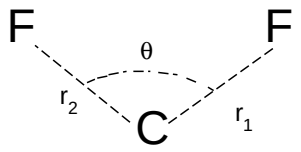

Figure 1: Molecule in internal coordinates.

A. Differential cross section

The fixed-nuclei differential cross section is computed and shown in Figure 2 in comparison to experiment and other calculations. In order to compare to the previous calculations, our results are shown without the Born correction. Since the experiment could not be performed below 20° and the effect of the dipole moment will become significant below 10° the differential cross sections plotted should be reliable. As can been seen in the figure, there is very good agreement between the two calculations and the experiment. The static exchange results of the previous calculation [11] and our static exchange calculations can not be distinguished on the figure so only ours are shown. Adding polarization to the calculation lowers the cross section in the forward direction. As the energy increases the effect of polarization decreases. The differences between the two calculations and the experiment may be due to changes in the differential cross section as a function of nuclear geometry. The calculations shown are at fixed geometry. These results should be averaged over the initial target vibrational wave function. The effect is usually small, but in this case the resonance becomes bound in the Franck-Condon region. In order to see the magnitude of the change we repeated these calculations for a range of angles and bond distances. Figure 3 shows the effect of changes in these parameters. As can be seen, the cross section in the forward direction is quite sensitive to changes in the internuclear separation and the bend. These results show that the relaxed SCF calculation gives a good description of the electron scattering in the low energy region. Therefore, the calculations of the resonant surfaces were done at this level.

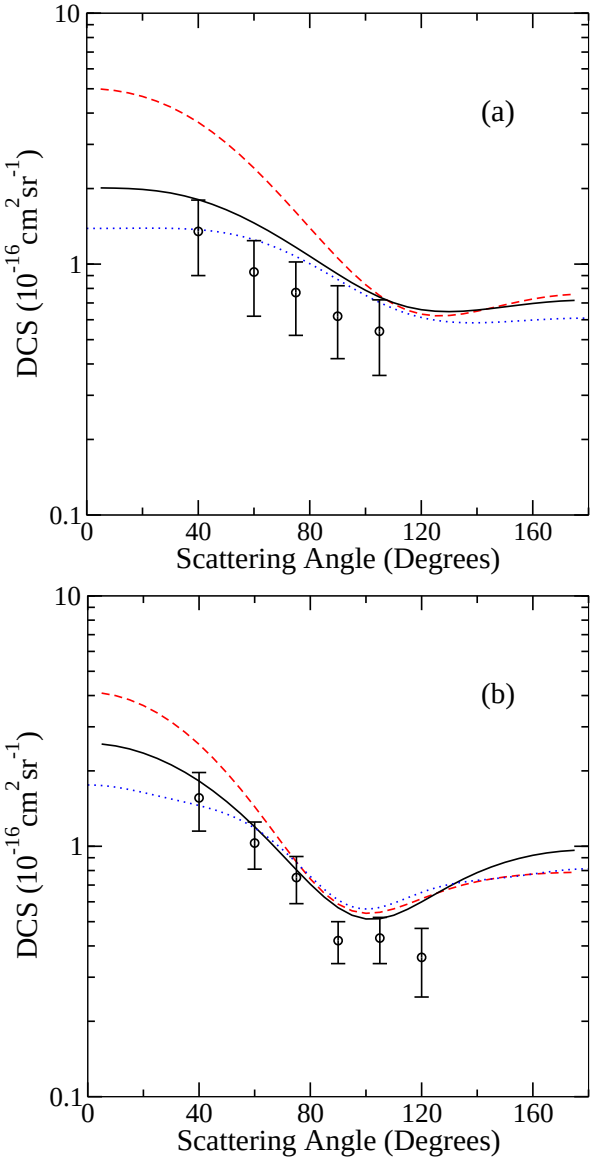

Figure 2: Differential cross section for electron scattering from CF_2 at (a) 3.0 eV and (b) 6.0 eV. The results at the static exchange level are shown with dashed lines (red on-line), while the solid black lines show the results at the RSCF level. Results from previous calculations [11] and experiment [11] are displayed with the dotted (blue on-line) lines and symbols respectively.

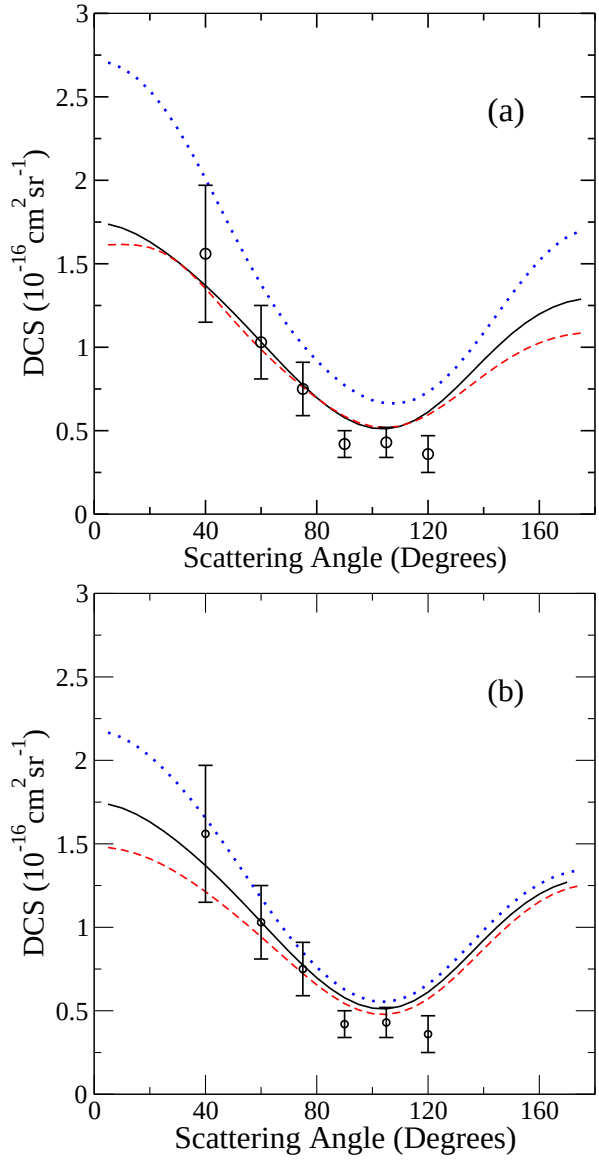

Figure 3: (a) Effect of changing the C–F bond distance on the differential cross section $\theta = 104.8°$, one C–F bond fixed at $r_1 = 2.4$ a$_0$ and the second at $r_2 = 2.3$ a$_0$ dashed line (red on-line), $r_2 = 2.4$ a$_0$ solid black line and $r_2 = 2.6$ a$_0$ dotted line (blue on-line). (b) Molecule bending effect on the differential cross section for $r_2 = 2.4$ a$_0$ and angle θ fixed at 100° dashed line (red on-line), 104.8° solid black line, and 110° dotted line (blue on-line).

B. Resonance surface

The computation of the eigenphase sums as a function of incident electron energy reveals one low-lying shape resonance. In Figure 4 the eigenphase sum show the resonance feature of CF_2 in $^2A''$ symmetry up to an electron collision energy of 0.2 Hartrees (5.44 eV). Figure 4a displays the effect of changing the C-F bond, while keeping the angle fixed at the equilibrium geometry, $\theta = 104.8°$ and the other C-F bond at 2.4 a$_0$. As can been seen in the figure, the resonance moves to lower energy and becomes bound as the bond distance is increased. Figure 4b shows the effect of bending at fixed bond distances. The eigenphase sums shown in the figure were calculated at the bond distances fixed at $r_1 = r_2 = 2.0$ a$_0$, where the resonance is not bound. As can be seen in the figure, the resonance energy position is much less sensitive to the bend angle. The potential energy used in our calculations is expressed in the (r_1, r_2, θ) coordinates spanning the domain [1.6 a$_0$, 8.0 a$_0$] × [1.6 a$_0$, 8.0 a$_0$] × [80°, 160°].

For comparison, a one dimensional cut of the potential

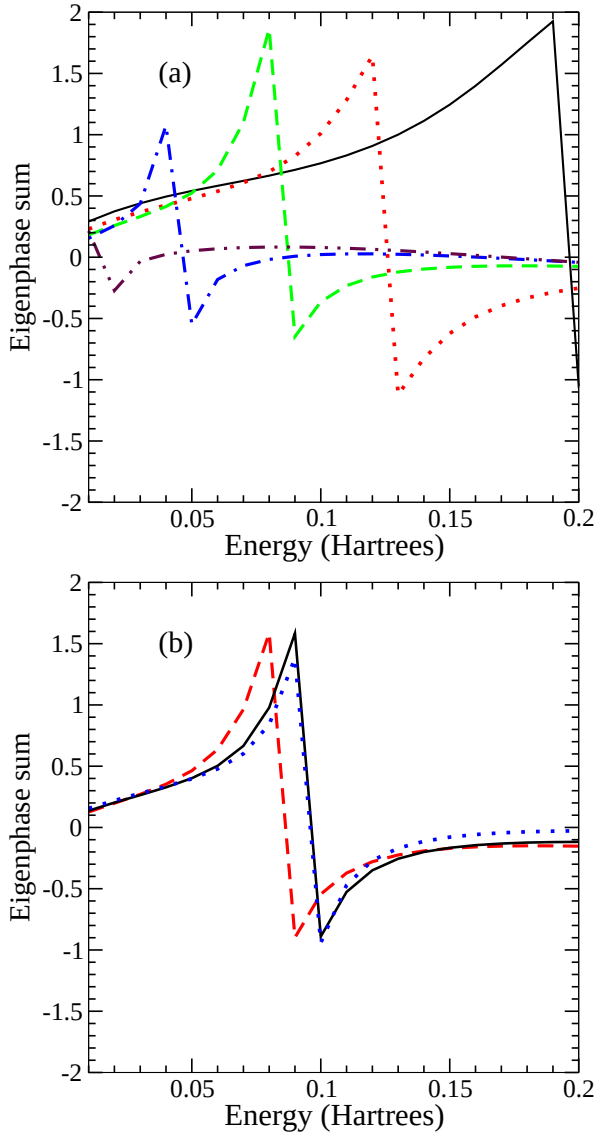

Figure 4: (a) Effect of changing the C–F bond distance on the eigenphase sum θ fixed at 104.8° and one C–F bond fixed at $r_1 = 2.4$ a$_0$ and $r_2 = 1.4$ a$_0$ black solid line, $r_2 = 1.6$ a$_0$ dotted line (red on-line), $r_2 = 1.8$ a$_0$ dashed line (green on-line), $r_2 = 2.0$ a$_0$ dot-dashed (blue on-line) and $r_2 = 2.3$ a$_0$ dot-dot-dashed (magenta on-line). (b) Molecule bending effect on the eigenphase sums for $r_1 = r_2 = 2.0$ a$_0$ and angle θ fixed at 90° dashed line (red on-line), 104.8° solid black line, and 120° dotted line (blue on-line).

energy surfaces of the ground state of the neutral CF_2 and the anion CF_2^- at the static-exchange level and the RSCF level are shown in Figure 5 as a function of r_2 with r_1 fixed at 2.4 a$_0$ and the angle θ fixed at 104.8°. The dissociation energy for the ground state is found to be 0.25 Hartrees (6.8 eV) in fair agreement with the measured value in [18]. The anion surface at the RSCF crosses the neutral at a bond distance smaller than the equilibrium bond distance of the neutral.

As a function of angle, both for the ground state of the

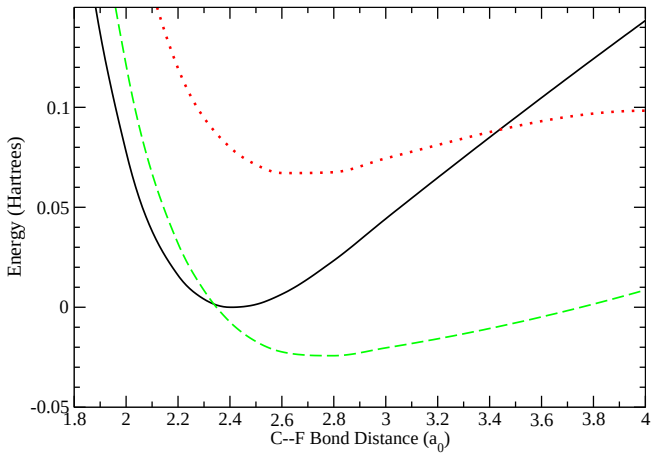

Figure 5: One dimensional cut of the potential energy surfaces of the ground state of the neutral CF_2 solid black line and the ground state of the anion CF_2^- at the static-exchange level dotted line (red on-line) and the relaxed SCF level dashed line (green on-line) as a function of r_2 with r_1 fixed at 2.4 a$_0$ and the angle θ fixed at 104.8°.

neutral and the anion surfaces show little change. One-dimensional cuts for several angles are shown in Figure 6a for the neutral and Figure 6b for the anion at the RSCF level as a function of r_2 with r_1 fixed at 2.4a$_0$. There is a much stronger variation with change in the bond distance. One-dimensional cuts for several values of r_1 are shown in Figure 7a for the neutral and Figure 7b for the anion at the RSCF level with the angle θ fixed at 104.8°.

Similar behavior is seen for the autoionization width, shown in Figure 8. There is little variation with angle, but a stronger change with internuclear separation.

III. NUCLEAR DYNAMICS

We solve for the nuclear dynamics of the metastable negative ion state in the local complex potential model. The approximation used in this model has been discussed in detail elsewhere [19] and will only be outlined here. The nuclear wave equation is given by:

$$[E_{tot} - \hat{H}(\mathbf{Q})]\xi_\nu(\mathbf{Q}) = \eta_\nu(\mathbf{Q}), \tag{4}$$

where the Hamiltonian operator is given by:

$$\hat{H}(\mathbf{Q}) = \hat{T}_Q + V_{el}(\mathbf{Q}), \tag{5}$$

The kinetic energy operator $\hat{T}_Q$ for a total momentum operator $J = 0$ is given in the (r_1, r_2, θ) coordinate sys-

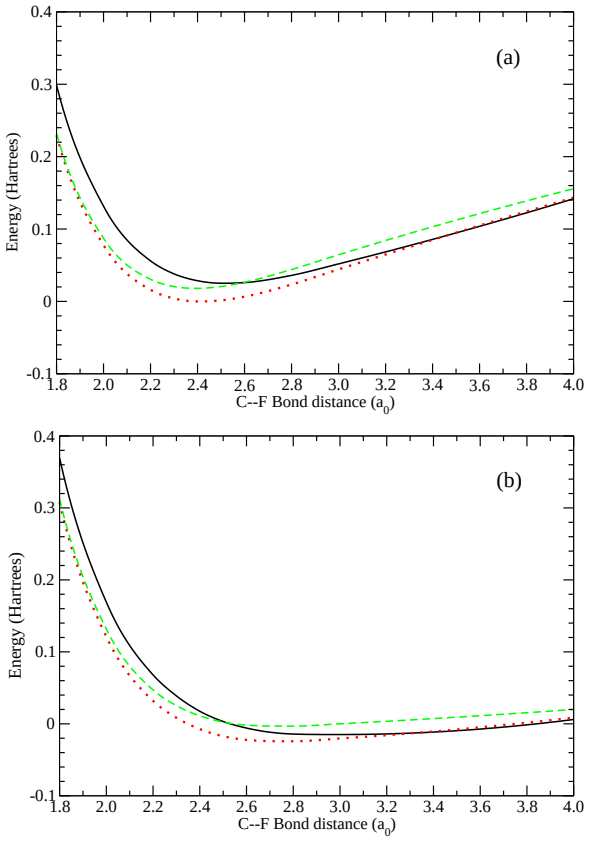

Figure 6: Potential energy surfaces of the ground state of the neutral CF_2 (a) and the anion CF_2^- (b) as a function of r_2, r_1 fixed at 2.4 a_0 for three values of θ: 90.0° black solid line, 104.8° dotted line (red on-line) and 120.0° dashed line (green on-line).

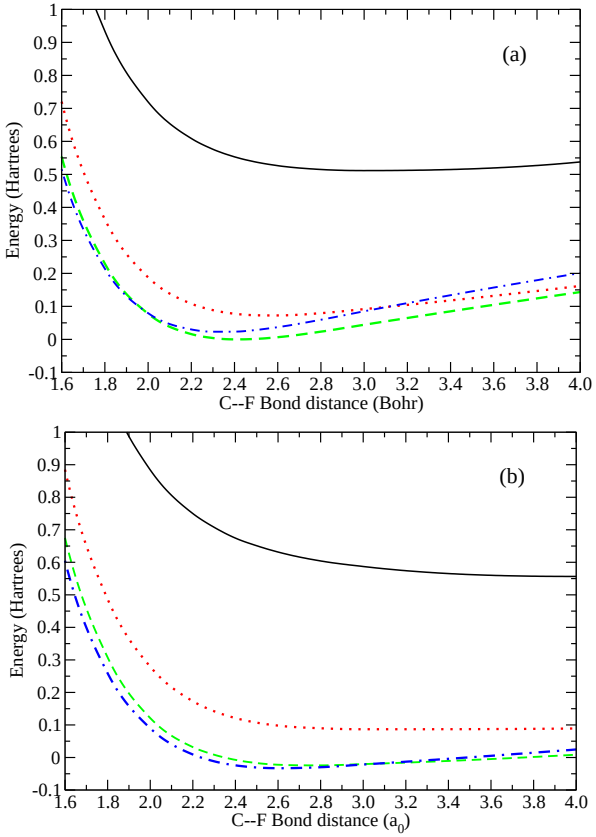

Figure 7: Potential energy surfaces of the ground state of the neutral CF_2 (a) and the anion CF_2^- (b) as a function of r_2, θ fixed at 104.8° for four values of r_1: 1.6 a_0 black solid line, 1.8 a_0 dotted line (red on-line), 2.4 a_0 dashed line (green on-line) and 2.8 a_0 dashed-dot line (blue on-line).

tem by:

$$\hat{T}_Q = -\frac{1}{2\mu_1}\partial_{r_1}^2 - \frac{1}{2\mu_2}\partial_{r_2}^2 + \left(\frac{1}{2\mu_1 r_1^2} + \frac{1}{2\mu_2 r_2^2}\right)\hat{j}^2 - \frac{1}{2m_C}\partial_{r_1}\partial_{r_2} + \frac{1}{m_C}\left(\frac{1}{r_1}\partial_{r_2} + \frac{1}{r_2}\partial_{r_1}\right)\partial_\theta \sin(\theta) - \frac{1}{2m_C r_1 r_2}\left[\cos(\theta)\hat{j}^2 + \hat{j}^2\cos(\theta)\right], \quad (6)$$

where $\mu_1 = \mu_2 = \left(\frac{1}{m_F} + \frac{1}{m_C}\right)^{-1}$ defines the reduced masses associated with r_1 and r_2 with m_C and m_F being the masses of the carbon and fluoride atoms respectively. The operator $\hat{j}^2$ in Eq. (6) represents the angular momentum operator squared. (Note that we use atomic units $\hbar = m_e = 1$ throughout). The complex potential $V_{el}(\mathbf{Q})$ relevant to the resonant CF_2^- anion is defined by

$$V_{el}(\mathbf{Q}) = E_{el}(\mathbf{Q}) + \epsilon_{res}(\mathbf{Q}) - \frac{i}{2}\Gamma(\mathbf{Q}). \quad (7)$$

The driving term $\eta_\nu(\mathbf{Q})$ in Eq. (4) is known as the "entry amplitude" and it expresses the capture probability of the incoming electron by the molecular target in the discrete vibrational state $\chi_\nu(\mathbf{Q})$ into the resonant state associated with the complex potential of Eq. (7). In our model, it is expressed as

$$\eta_\nu(\mathbf{Q}) = \left(\frac{\Gamma(\mathbf{Q})}{2\pi}\right)^{1/2}\chi_\nu(\mathbf{Q}). \quad (8)$$

Finally, $\xi_\nu(\mathbf{Q})$ is the nuclear wave function we seek to determine. We use the time-dependent formulation established by McCurdy and Turner [20]. The problem thus reduces to solving the time-dependent Schrödinger equation.

$$\begin{cases} \hat{H}(\mathbf{Q})\Phi_{nuc}(\mathbf{Q},t) = i\partial_t\Phi_{nuc}(\mathbf{Q},t); \\ \Phi_{nuc}(\mathbf{Q},0) = \eta_\nu(\mathbf{Q}) \end{cases} \quad (9)$$

We use the computational technique based on MCTDH formalism discussed in detail in [21]. In the context of this theory, the nuclear wave function for the negative ion of CF_2 is expressed in the internal coordinates as

$$\Phi_{nuc}(r_1, r_2, \theta, t) = \sum_{i,j,k}^{N_r,N_r,N_\theta} A_{ijk}(t) w_{i,j,k}(r_1, r_2, \theta, t), \quad (10)$$

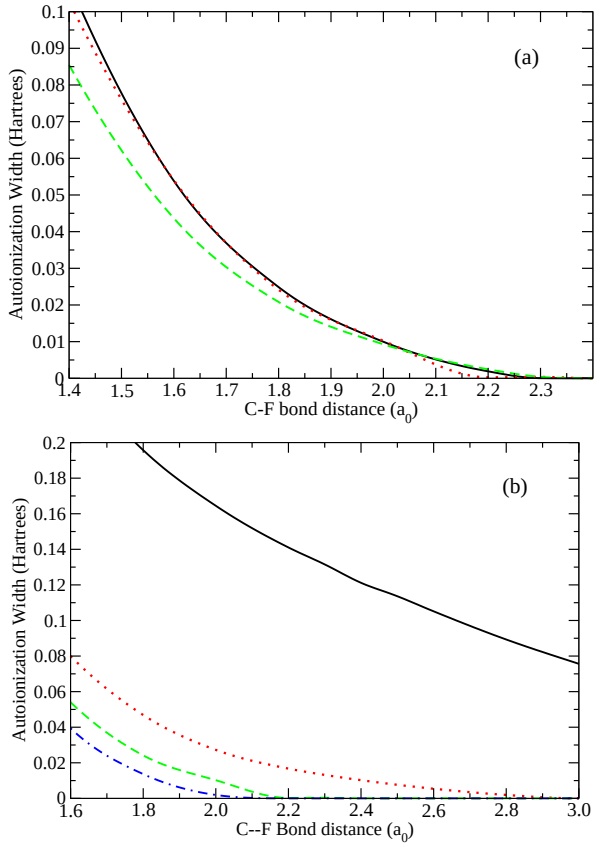

Figure 8: (Color online) Autoionization width: (a) as a function of r_2, r_1 fixed at 2.4 a_0 for three values of θ 90.0°, black solid line, 104.8°, dotted line (red on-line) and 120.0°, dashed line (green on-line). (b) as a function of r_2, θ fixed at 104.8° for four values of r_1, black solid line, 1.6 a_0, dotted line (red on-line) 1.8 a_0, dashed line (green on-line) 2.4 a_0 and dashed-dot line (blue on-line) 2.8 a_0.

where

$$w_{i,j,k}(r_1, r_2, \theta, t) = \rho_i^1(r_1, t)\rho_j^2(r_2, t)\Theta_k(\theta, t). \qquad (11)$$

Each single-particle function appearing in Eq. (11) is in turn expanded in terms of a function basis set chosen to correspond to that of a Discrete Variable Representation (DVR) for computational efficiency. Here, $N_{r_1} = N_{r_2} = 30$ and $N_\theta = 8$. The single-particle functions associated with the variables r_1 and r_2 are expressed in terms of sine-DVR (300 grid points each) and the angle θ is represented by the Legendre-DVR (66 grid points).

IV. COMPUTATIONAL RESULTS

The wavepacket for the ground neutral state is computed by relaxation, that is, propagation on the neutral adiabatic potential energy surface in negative imaginary time. By applying Eq. (8), we determine the initial wavepacket needed to solve the system of equation Eq. (9).

At the grid boundaries, an appropriate complex absorbing potential (CAP) is included to ensure that wavepacket is not reflected back into the grid causing undesired interferences. The form of the CAPs adopted in this study is given by the form

$$-iW(R) = -iC|R - R_{CAP}|^b S(R - R_{CAP}), \qquad (12)$$

where S is the Heaviside step function and the values of the parameters C, b and R_{CAP} used in this propagation are 0.01, 3.0 and 5.0 a_0, respectively. Propagation is carried out for a duration of 1000 fs.

A. Cross section

The wavepacket flux at the grid boundaries is used to compute the DEA cross section. The energy-resolved outgoing flux associated with the initial target vibrational state ν through the CAP is therefore given by

$$F_\nu(E) = \frac{1}{(2\pi)^2|\Delta(E)|^2}\left\langle \xi_\nu \left| \widehat{F} \right| \xi_\nu \right\rangle_{\mathbf{Q}}, \qquad (13)$$

where $\widehat{F}$ is the flux operator and $\Delta(E)$ is the energy distribution of the initial [22] In order to achieve a time-dependent dynamics formulation of the process, the bracket term in Eq. (13) is computed in terms of the time domain integrals as:

$$\left\langle \xi_\nu \left| \widehat{F} \right| \xi_\nu \right\rangle_{\mathbf{Q}} = \qquad (14)$$

$$\int_0^\infty dt \int_0^\infty dt' \left\langle \eta_\nu \left| e^{i(\widehat{\tilde{H}}^\dagger - E)t} \widehat{F} e^{-i(\widehat{\tilde{H}} - E)t'} \right| \eta_\nu \right\rangle_{\mathbf{Q}},$$

where the operator $\widehat{\tilde{H}}$ is given by

$$\widehat{\tilde{H}} = \widehat{H} - iW(R), \qquad (15)$$

representing the CAP-perturbed Hamiltonian of the system defined in Eq. (5).

The cross section relevant to the DEA channel for an initial neutral target in the vibrational mode ν may be expressed based on the flux function as

$$\sigma_{\nu \to DEA}(\frac{k^2}{2}) = g_s g_a \frac{4\pi^3}{k^2} F_\nu(\frac{k^2}{2}), \qquad (16)$$

where g_s is the statistical ratio of the electronic multiplicity of the resonant state to the electron multiplicity of the neutral target (here equal to 2) and g_a is the arrangement multiplicity (here equal to 1). The reader is referred to Ref [22–25] for detailed treatment of the CAP-based flux formalism.

In Figure 9, the DEA cross section at the RSCF level is shown for a one-dimensional (θ and one C–F bond fixed), two-dimensional (θ fixed) and three-dimensional calculations. In the one-dimensional calculation, the electron

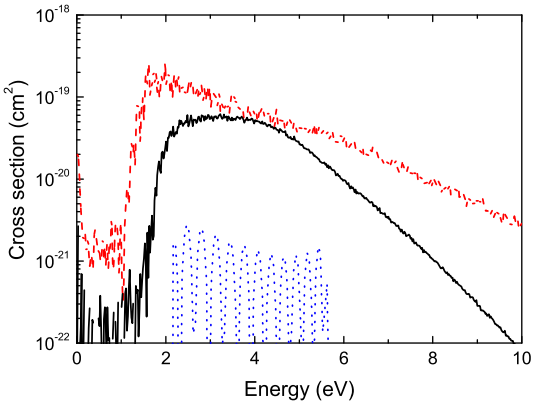

Figure 9: DEA cross section for F^- production from CF_2 with resonance parameters determined at the RSCF level, one-dimensional - dotted line (blue on-line) - r_1 as variable, θ and r_2 fixed; dashed line (red on-line) two-dimensional surface - r_1 and r_2 as variables, θ fixed; full three-dimensional surface black solid line

can be captured at low collision energy, however, the anion state is not open for dissociation until the energy is larger than 2 eV. It is the high-energy tail of the capture probability that has enough energy for dissociation. The cross section calculated within the 1D model, is very small (10^{-21} cm^2) with regular oscillations due to energy-dependent overlap between the vibrational wavefunction of the target molecular and the continuum function of the anion [26, 27]. In two dimensions, the peak of the cross section occurs around 3 eV and with a peak height of roughly $1 \cdot 10^{-19}$cm^2. However, when the bend is added the cross section drops. Bending does not lead to dissociation, so as the wave packet spreads in that dimension it can only autoionize. We obtain a peak value of $6 \cdot 10^{-20}$ cm^2 at around 2 eV. This is consistent with the estimate given by Graupner *et al.* [13] which put an upper limit on the DEA cross section of less than $5 \cdot 10^{-20}$ cm^2 for energies less than 10 eV and the observations of Shuman *et al.* [14] that observed no attachment in this system over a similar energy range.

In the experiments [13] the temperature was 300 K. The vibrational frequencies are: symmetric stretch,152 meV, asymmetric stretch, 138meV, and bend, 82 meV [28]. Therefore the symmetric and asymmetric stretches are in the ground vibrational states. The lower frequency bend has a population of 4% in $\nu = 1$ and 96% in $\nu = 0$. In order to assess the effect of vibrational excitation, a calculation was carried out with excitation in the bend. The results are shown in Figure 10. The cross section increases with increasing vibrational excitation, but by $\nu = 3$ it is only a factor of ten higher. This will not lead to any significant changes the dissociative electron attachment rate.

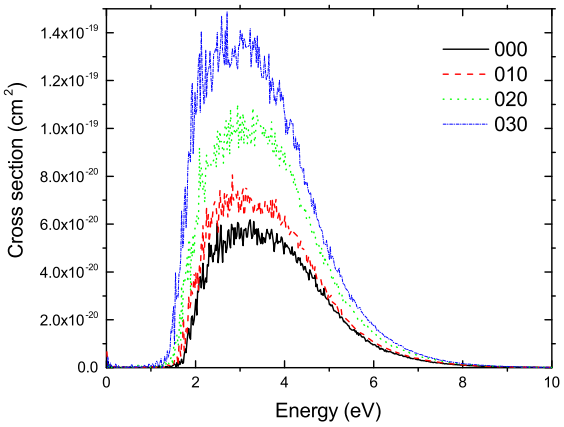

Figure 10: DEA cross section for F^- production from CF_2 as a function of initial vibrational excitation in the bending mode, $\nu = 0$ solid line (black on-line), $\nu = 1$ dashed line (red on-line), $\nu = 2$ dotted line (green on-line), $\nu = 3$ dot-dashed line (blue on-line).

V. CONCLUSION

We have carried out theoretical calculations on DEA of CF_2. These calculations show that the resonance that appears at the static-exchange calculations at the equilibrium geometry becomes bound when polarization effects are included. The DEA cross section is found to be quite small, in agreement with the most recent experiments. This means, as previously speculated [8, 10], that DEA of CF_2, as was found with our previous studies of DEA of CF can not be a source of F^- in processing plasmas. Further work is needed to study, for example, DEA of CF_3, to see if this system could be a source, although recent experiments [14] indicate this is inefficient. Another possible source is the ion-pair channel in the dissociative recombination of CF^+, the process:

$$CF^+ + e^- \rightarrow C^+ + F^-$$

Further work is needed to test this possibility.

VI. ACKNOWLEDGMENTS

We acknowledge support from the National Science Foundation under Grant No.PHY-11-60611. AEO acknowledges support by the National Science Foundation, with some of this material based on work while serving at NSF. Å L acknowledges support from the Swedish Research Council and the Carl-Trygger Foundation.

[1] L. G. Christophorou and J. K. Olthoff, Appl. Surf. Sci. **192**, 309326 (2002).

[2] L. G. Christophorou and J. K. Olthoff, *Fundamental Electron Interactions with Plasma Processing Gases* (Kluwer Academic/Plenum, New York, 2004).

[3] S. Samukawa, T. Mukai, and Noguchi, Mater. Sci. Semcond. Process **2**, 203 (1999).

[4] V. Georgieva, A. Bogaerts and R. Gijbels, J. Appl. Physics **94**, 3748 (2003).

[5] K. Denpoh and K. Nambu, Japan. J. Appl. Physics **39**, 2804 (2000).

[6] M. J. Kushner, *Database Needs for Modeling and Simulation of Plasma Processing*, (National Research Council, Washington, DC, 1996).

[7] I. Rozum, N. J. Mason and J. Tennyson, J. Phys. B **35**, 1583 (2002).

[8] I. Rozum, P. Limão-Vieira, S. Eden, J. Tennyson and N. J. Mason, Phys. Chem. Ref. Data **35**, 267 (2006).

[9] C. S. Trevisan, A.E. Orel, and T. N. Rescigno Phys. Rev. A **72**, 062720 (2005).

[10] I. Rozum and J. Tennyson, J. Phys. B **37**, 957 (2004).

[11] J. R. Francis-Staite, T. M. Maddern, M. J. Brunger, S. J. Buckman, C. Winstead, V. McKoy, M. A. Bolorizadeh and H. Cho, Phys. Rev. A **79**, 052705 (2009).

[12] R. L. Schwartz, G. E. Davico, T. M. Ramond and W. C. Lindberger, J. Phys. Chem **103**, 8213 (1999).

[13] K. Graupner, T. Field, and C. A. Mayhew, New Journal of Physics **12**, 083035, (2010).

[14] N. S. Shuman, T. M. Miller and A. A. Viggiano, J. Chem. Phys. **137**, 214318 (2012)

[15] T. N. Rescigno, B. H. Lengsfield, and C. W. McCurdy, in *Modern Electronic Structure Theory*, edited by D. R. Yarkony (World Scientific, Singapore, 1995), Vol. **1**, p. 501.

[16] S. Geltman, "*Topics in Atomic Collision Theory*" (Academic Press, 1997) p. 31.

[17] T. H. Dunning, Jr. and P. J. Hay in *Methods of Electronic Structure Theory* edited by H. F. Schaefer III (Plenum Press, N.Y., 1977), p. 1-27.

[18] JANAF thermochemical tables. In: D.R. Stuhl and H. Prophet, Editors, J. Phys. Chem. Ref. Data **1**4 (1985) suppl. 1 .

[19] T. F. O'Malley, Phys. Rev. **150**, 14 (1966).

[20] C. W. McCurdy and J. L. Turner, J. Chem. Phys. **78**, 6773, (1983).

[21] G. A. Worth, M. H. Beck, A. Jäckle, and H.-D. Meyer, MCTDH package, Version 8.4 (2007); See *http://www.pci.uni-heidelberg.de/tc/usr/mctdh/*.

[22] A. Jäckle and H.-D. Meyer, J. Chem. Phys. **105** 6777 (1996).

[23] M. H. Beck, A. Jäckle, G. A. Worth and H.-D. Meyer, Physics Reports **324**, 1(2000).

[24] H.-D. Meyer and G. A. Worth, Theor. Chem. Acc. **109**, 251 (2003).

[25] U. V. Riss and H.-D. Meyer,Phys. B: At Mol. Opt Phys. **26**, 4503 (1993).

[26] O. Motapon, M. Fifirig, A. Florescu, F. O. Waffeu Tamo, O. Crumeyrolle, G. Varin-Bréant, A. Bultel, P. Vervisch, J. Tennyson, and I. F. Schneider, Plasma Sources Sci. Technol. **15**, 23 (2006).

[27] J. B. Roos, Å. Larson and A. E. Orel, Phys. Rev. A **78**, 022508 (2008).

[28] H. B. Qian and P. B. Davies, J. Mol. Spectrosc. **169** 201.